EIGHTEENTH EUROPEAN ROTORCRAFT FORUM

B . 08

Paper N° 2

ON A FINITE-STATE INFLOW APPLICATION TO
FLAP-LAG-TORSION DAMPING IN HOVER

Donizeti de Andrade

Assistant Professor, Divisão de Engenharia Aeronáutica
Instituto Tecnológico de Aeronáutica
Centro Técnico Aeroespacial
12228 São José dos Campos, S.P., Brasil

David A. Peters

Professor, Department of Mechanical Engineering
Washington University
St. Louis, MO 63130, U.S.A.

September 15-18, 1992

AVIGNON, FRANCE

ASSOCIATION AERONAUTIQUE ET ASTRONAUTIQUE DE FRANCE

ON A FINITE-STATE INFLOW APPLICATION TO FLAP-LAG-TORSION DAMPING IN HOVER

Donizeti de Andrade

Assistant Professor, Divisão de Engenharia Aeronáutica
Instituto Tecnológico de Aeronáutica - Centro Técnico Aeroespacial
12228 São José dos Campos, S.P., Brasil

and

David A. Peters

Professor, Department of Mechanical Engineering
Washington University
St. Louis, MO 63130, U.S.A.

ABSTRACT

The aeroelastic stability of helicopter rotors in hovering flight is investigated by a coupled set of generalized dynamic wake equations and hybrid equations of motion for an elastic blade cantilevered in bending and having a torsional root spring to model pitch-link flexibility. The inflow states are governed by a system of first-order, ordinary differential equations in time, with the pressure distribution at the rotor disk expressed as a summation of the discrete loading on each blade, accounting simultaneously for a finite number of blades and overall rotor effects. The blade equations are simplified by the assumption of uniform blade mass and stiffness; and then they are reduced to nonlinear differential equations by Galerkin's method. The coupled model establishes nonlinear algebraic equations for the equilibrium/steady-state problem, and a standard eigenanalysis for the stability of small motions about the equilibrium condition. The model has been applied to a two-bladed, untwisted, stiff inplane hingeless small scale rotor with torsionally soft blades, including a blade root offset, and hub designed to permit variation in precone, blade droop, pitch control stiffness, and blade pitch angle. Overall results from this research, reinforce qualitative and quantitative shortcomings associated with quasi-steady two-dimensional aerodynamic theory for aeroelastic applications in hover, and set the present finite-state methodology as a suitable tool to handle helicopter integrated dynamics. This is chiefly due to elimination of time-marching and moving block analyses inherent to previous approaches to the same problem, implying in substantial savings in computer memory and time, with no essential loss of accuracy. This more efficient strategy opens the way for efficient optimization of rotor blades with treatment of aeroelastic stability.

Nomenclature

a_n^m, b_n^m	induced flow expansion coefficients in the rotating frame, nondimensional
B_{nl}^m	$= (-1)^{(n+l-2m-2)/2} \sqrt{\dfrac{K_n^m}{K_l^m}} \sqrt{2n+1} \sqrt{2l+1} \displaystyle\sum_{q=m,\,m+2,\dots}^{n-1} \dfrac{\pi}{2} K_q^m \dfrac{(2q+1)}{(l-q)(l+q+1)}$
K_n^m	$= \dfrac{2}{\pi} \dfrac{(n+m-1)!!\,(n-m-1)!!}{(n+m)!!\,(n-m)!!}$
m, n	harmonic and shape function numbers, respectively
N	number of modified orthogonal Duncan polynomials in blade modal expansions for each of the elastic torsion, flap bending, and lead-lag bending deflections
Q	number of rotor blades
R	rotor radius, m
$\bar{r}$	blade radial coordinate, $\bar{r} = r / R$,
$\bar{t}$	nondimensional time, $\bar{t} = \Omega\,t$
U_∞	free-stream velocity component of the blade section, m/s
y', z'	blade coordinates associated with the deformed blade reference frame, along unit vectors $\underline{j}', \underline{k}'$
$\bar{\lambda}$	induced flow at the rotor disk due to shed wake, positive downwards, $\bar{\lambda} = \lambda /(\Omega R)$
$\phi_n^m(\bar{r})$	$= \sqrt{(2n+1)\dfrac{\pi}{2} K_n^m} \displaystyle\sum_{q=m,\,m+2,\dots}^{n-1} \bar{r}^q \dfrac{(-1)^{(q-m)/2}(n+q)!!}{(q-m)!!\,(q+m)!!\,(n-q-1)!!}$
Ω	rotor rotational speed, rad/s
$(\,)^*$	$= d/d\bar{t}$

1. Introduction

The physical behavior of helicopter rotor blades has been investigated for many years. At this time, it is well known that a continuous pumping of a substantial mass of air (inflow) through the rotor disk (due to the existence of a shed wake below the helicopter rotor) implies that its aerodynamic field, in hovering or forward flight, is very different and much more complicated than its fixed-wing counterpart. A suitable wake model is necessary not only for performance predictions (which, in general, rely on average values of the wake geometry corresponding to a given configuration and operating condition) but also for any study involving rotor dynamics, as is the case in aeroelastic analysis. The advent of hingeless rotors with very flexible blades has made even stronger the already inherent coupling of the aerodynamic and structural dynamic loads acting upon helicopter rotor blades. Coexisting in a strongly fluctuating aerodynamic environment, the elastic deformations contribute to changes in both the aerodynamic and structural loads acting on the blades, characterizing an aeroelastic phenomenon. The aeroelastic environment of the helicopter rotor can be modeled as shown in the flow-chart in Figure 1. At least three basic technology modules must be coupled within an aeroelastic analysis of the helicopter rotor [1]: 1) a structure dynamic model, 2) a induced flow model, and 3) an airloads model. The double feedback loop emphasizes the important coupling between dynamic inflow and rotor dynamics through the predicted airloads, that become the forcing functions for both the structure and the induced flow.
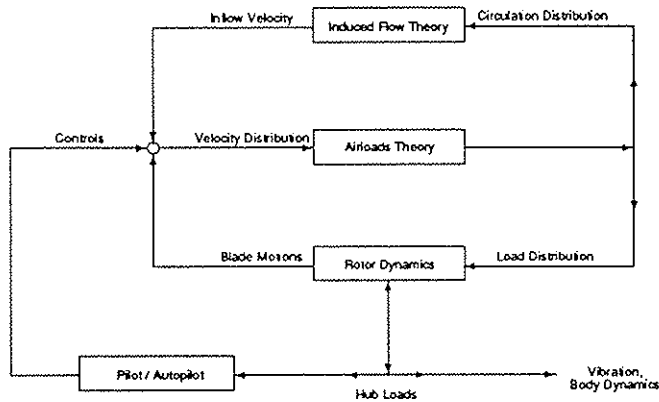

Figure 1. Aeroelastic Environment of the Helicopter Rotor.

Classically, the aeroelastic problem of rotor blades in hovering flight has been approached in two distinct ways: 1) analyses presenting either a relatively sophisticated structural dynamic model combined with simple, quasi-steady, two-dimensional aerodynamic theory, or, 2) analyses with an elaborate free-wake approach in connection with a simple rigid blade structural model. Neither approach leads to consistent insight into the complex aeroelastic phenomenon described before. With respect to the induced flow model, it has been treated with a two-dimensional, quasi-steady aerodynamics, including a uniform induced flow distribution [2,3]. That modeling lacks some physical information, such as three-dimensional tip relief and unsteady wake vortex alignment, which are very important in predicting aerodynamic damping. A much more realistic approach would involve three-dimensional, unsteady aerodynamics, for which global effects and time-history of circulation would be taken into account.

More recently, research work has attempted to bridge the critical gap between structural and aerodynamic operators used in aeroelastic applications such as those in References [2,3]. In References [4,5], a panel code is formulated and coupled, respectively, with the nonlinear blade models of References [2] and [3] (both based on the original Hodges and Dowell equations [6]). This panel model is based on a piecewise constant distribution of source and doublets, with a prescribed tip-vortex geometry and calculated inner wake. Results showed the importance of tree-dimensional and unsteady effects in the prediction of lead-lag damping. Due to the nature of the aerodynamic model used, where the aerodynamic forces and moments are expressed as complex nonlinear implicit functions of the blade deflections and motion, in the perturbation analysis the resulting generalized forces can not be linearized explicitly, excluding an ordinary eigenvalue analysis. A Fourier analysis associated with a moving block technique is employed to obtain damping and frequency of the most lightly damping mode, which has the frequency near the fundamental lead-lag bending frequency of the rotating blade. The fact that a standard eigenanalysis is out of the question (meaning that only the damping and frequency of the most lightly damped mode can be obtained) and that excessive computer memory requirements are inevitable to accomplish convergence (since small time steps and many wake layers underneath the rotor must be suitably established) imposes innate limitations to the use of this method in aeroelastic stability investigations.

Under the present approach the generalized dynamic wake model developed by Peters and He [7,8] is coupled with Hodges nonlinear blade model [3]. This blend is done in a way such the aerodynamic forces and moments in the blade equations, as well as the pressure coefficients in the generalized dynamic inflow equations, are obtained as explicit nonlinear functions of the blade deformation and generalized dynamic inflow state variables, leading to a standard eigenanalysis. Consequently, reliable and computationally efficient results are expected, which would validate the generalized dynamic wake methodology as an appropriate alternative to use in rotor design and optimization.

2. Generalized Dynamic Wake Equations in the Rotating System

The generalized dynamic wake equations formulated by Peters and He [7,8] are derived from the basic potential flow conservation laws, where the spatial variation of pressure across the rotor is related to the variation of velocity at

the disk (i.e., to the fluid flow momentum flux) and to the acceleration of the fluid flow through linear matrix operators. Particularized for hovering flight and written in the rotating system, they are given as

$$
\begin{bmatrix} \ddots & & \\ & \left[K_n^m\right] & \\ & & \ddots \\ & & & \left[K_n^m\right] \\ & & & & \ddots \end{bmatrix} \begin{Bmatrix} \vdots \\ \left\{a_n^m\right\} \\ \cdots \\ \vdots \\ \left\{b_n^m\right\} \\ \vdots \end{Bmatrix}^{*} + \begin{bmatrix} \ddots & & & \\ & \left[B_{nt}^m\right]\left[V_n^m\right] & & -m\left[K_n^m\right] & \\ & & \ddots & & \ddots \\ & m\left[K_n^m\right] & & \left[B_{nt}^m\right]\left[V_n^m\right] & \\ & & & & \ddots \end{bmatrix} \begin{Bmatrix} \vdots \\ \left\{a_n^m\right\} \\ \cdots \\ \vdots \\ \left\{b_n^m\right\} \\ \vdots \end{Bmatrix} = \frac{1}{2} \begin{Bmatrix} \vdots \\ \left\{\hat{\tau}_n^{mc}\right\} \\ \cdots \\ \vdots \\ \left\{\hat{\tau}_t^{ms}\right\} \\ \vdots \end{Bmatrix} \quad (1)
$$

Such a set of first-order differential equations is based on a nondimensional induced flow distribution at the rotor disk expanded in a entire set of harmonic and radial shape functions, including undetermined time dependent coefficients as aerodynamic states:

$$
\bar{\lambda}\,(\bar{r}, \hat{\psi}, \bar{t}) = \sum_{m,n} \phi_n^m(\bar{r}) \left[a_n^m(\bar{t}) \cos(m\hat{\psi}) + b_n^m(\bar{t}) \sin(m\hat{\psi}) \right]
$$

This induced flow representation not only offers a complete description of the flow, which is suitable to incorporate three-dimensional effects, but also handles higher harmonic dynamics, by the truncation at any harmonic of interest.

Within the first and second terms on the LHS of Equation (1) one observes, respectively, the "apparent mass" and "quasi-steady" operators. The former is obtained in closed form and includes diagonal matrices as elements, and the latter has a very simple form for hovering flight, carrying symmetric and diagonal matrices as elements. In Equation (1), for the cosine part m assumes values 0, 1, 2, ... while for the sine part m has values 1, 2, 3, ... The pressure distribution at the rotor disk, as seen on the RHS of Equation (1), is modeled as a summation of the discrete loading on each blade, accounting simultaneously for a finite number of blades and overall rotor effects. For instance, the cosine part of the wake forcing functions has the form:

$$
\hat{\tau}_n^{mc} = \frac{1}{\pi} \sum_{q=1}^{Q} \left[\int_0^1 \phi_n^m(\bar{r}) \mathrm{Jo}(m\hat{b}) \frac{L_S}{\rho_\infty \Omega^2 R^3} \, d\bar{r} \right] \cos(m\hat{\psi}_q) \qquad m \neq 0 \quad (2)
$$

L_S is the total wake-generating circulatory lift at the blade section [1,6-8] which can be evaluated from a lift theory, and ρ_∞ is the air density (kg/m^3). The J_0 term arises from matching the present inflow model with Theodorsen's lift theory [1,9]. This is accomplished when a particular chordwise pressure distribution, which results in no induced flow on the airfoil due to bound vorticity, is applied with the inflow distribution defined in Peters' and He's model [7,8]. As discussed in Reference [1], when one deals with slender (high aspect-ratio) blades, it is reasonable to set J_0 to unity. This is equivalent to a lifting-line approximation for the lift and induced drag, with the inflow computed on the lifting-line. As a consequence, the nondimensional pressure expansion coefficients at the RHS of Equation (1) have their expressions simplified considerably. The present research is based on the above assumptions.

3. The Hingeless Rotor Blade Model and Blade Equations of Motion

Blade Configuration

The blade configuration adopted in this research is shown in Figure 2. The parameters of interest in this study are precone, β_{pc}, the inclination of the pitch change bearing with respect to the plane of rotation (positive upwards); droop, β_d, the inclination (positive downwards at zero pitch angle) of the blade segment outboard of the pitch change bearing; and blade root offset, e_1, the distance between the center of rotation and the root of the blade. The blade is cantilevered in bending, and the kinematics of the pitch-link connection between the outboard segment of the blade and the swashplate control system is modeled by a torsional root spring. The blade bending deflections v and w are defined parallel to and fixed to the sectional principal axes at the root end of the blade (along y and z axes), as shown in Figure 3. This means that the lead-lag (v) and flap (w) are inplane and out-of-plane displacements only at zero thrust condition, because the y direction is established chordwise after the rigid body rotations, including collective pitch at the root (θ_0) and the pitch due to root spring deformation ($\Phi(t)$), are taken. The axial deflection u and the blade elastic torsion deformation ϕ are also sketched in Figure 3.

Blade Equations of Motion

The rotor is treated in isolation; no couplings with helicopter body degrees of freedom are accounted for. The blade equations of motion are derived from Hamilton's Principle. The cross section structural and inertial properties are assumed doubly symmetric with respect to the blade cross section principal axes and no strain energy from restrained torsional warping is considered. Furthermore, in this research, mass axis, tension axis, and aerodynamic center offsets
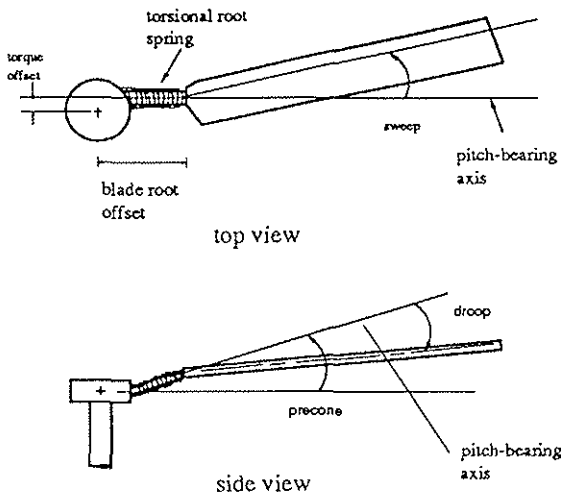
Figure 2. Rotor Blade Configuration.

from the elastic axis are all zero. The structural and inertial operators are taken from References [6] and [3], respectively.

The aerodynamic operator is based on thin airfoil theory, in a way such that it allows a time domain analysis, with a three-dimensional wake-induced flow governed by the generalized dynamic inflow model presented in Equation (1), according to the development presented in Reference [9]. The airfoil lift curve slope and profile drag coefficient are assumed constants. The blade section is pivoted at an axis at its quarter-chord point (i.e., the x' axis normal to y' and z' axes in Figures 4 and 5; it coincides with the blade elastic axis intersection at the airfoil and is also the airfoil aerodynamic center in the context of thin airfoil theory). The deformed blade section is pitching at an angular speed $\dot{\varepsilon}$ about x' axis, as shown in those figures. From Figure 4 it can be seen that the airfoil velocity components along the principal axes y' and z' (through the shear center of the section) are U_T $\underline{j}'$ and U_P $\underline{k}'$. α is the instantaneous angle of attack of the blade section and it is defined as the angle between the chordline and the resultant velocity at the cross section, $\underline{U} = U_T \underline{j}' + U_P \underline{k}'$. Also, the lift per unit of length (circulatory, L_C, and noncirculatory, L_{NC}) and pitching moment per unit of length (circulatory and noncirculatory) are expressed in terms of U_T, U_P and $\dot{\varepsilon}$. Since U_T, U_P and $\dot{\varepsilon}$ can be expressed in terms of the blade elastic displacements, v, w, and ϕ, the root pitch Φ, and the inflow expansion coefficients a_m^n and b_m^n, the generalized aerodynamic forces and moments, L_u, L_v, L_w, M_ϕ and the integral over the blade length of the moment due to the root spring, M_Φ, are expressed in terms of blade displacements and inflow expansion coefficients as well.

In the derivation of the blade equations a ordering scheme is employed, based on a small parameter of the order of magnitude of the bending slopes. Resulting equations are simplified by integration of the variational equation for the blade radial displacement to obtain the blade tension and by an expression of tension and radial displacements in terms of remaining blade displacements and torsional root spring deformation. In summary, a set of nonlinear hybrid equations of motion, consisting of one integro-partial differential equation for the root pitch, and three integro-partial differential equations each for flapwise and chordwise bending and elastic torsion, is obtained.

Figure 3. Orientation of Elastic Blade Displacements.

Concerning the airloads-inflow coupling, three points should be commented: 1) under the assumptions of the thin airfoil theory ($U \approx U_\infty$), and up to the second order, the wake-generating circulatory lift is taken as the circulatory part of L_w in this research (rigorously, one should take the circulatory lift normal to the rotor disk, along the induced flow direction, for all operational conditions; 2) a lifting-line approximation is taken by setting J_0 to unity in the nondimensional pressure expansion coefficients (Equations (1) and (2)) implies that effects of bound vorticity on the inflow are not eliminated [1]; and 3) under thin airfoil theory, the lifting line is placed at the blade quarter-chord, which, typically, has a constant azimuthal coordinate for a rectangular blade. Since $\widehat{\psi}_q$, the azimuthal position of the q-th blade, is defined at the blade midchord for the compatibilization with Theodorsen's lift theory [1,9], it would, rigorously, be a function of the radial coordinate, $\bar{r}$. However, numerical results from Reference [1] show that this skewing (yawing) has a negligible effect on the inflow computation.
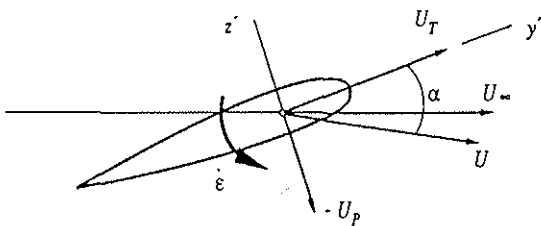

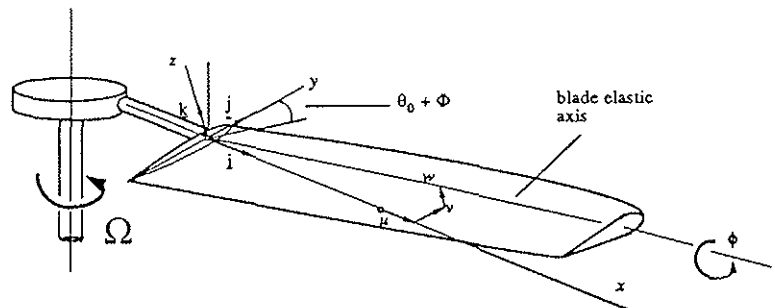
Figure 4. Unsteady Motion of the Blade Section.

4. Coupling Inflow and Blade Equations of Motion - Solution Approach

The first step towards solution is to simplify the blade nonlinear hybrid equations by the assumption of uniform mass and stiffness, and to obtain nonlinear ordinary differential equations in time by applying Galerkin's method.

Before applying Galerkin's method, the blade nondimensional displacements in lead-lag, flap (both nondimensional on $(R - e_1)$), and torsion are expanded, respectively, as

$$\bar{v} = \sum_{i=1}^{N} \left[V_{0i} + \Delta V_i \, (\bar{t}) \right] \Psi_i \, (\bar{x}) ; \qquad \bar{w} = \sum_{i=1}^{N} \left[W_{0i} + \Delta W_i \, (\bar{t}) \right] \Psi_i \, (\bar{x}) ; \qquad \phi = \sum_{i=1}^{N} \left[\Phi_{0i} + \Delta \Phi_i \, (\bar{t}) \right] \Theta_i (\bar{x})$$

Each expansion assumes small unsteady perturbation about steady equilibrium condition; the variables with "zero" indexes are equilibrium generalized coordinates, and the ones with "delta" are perturbation coordinates. Modified orthogonal Duncan polynomials are taken as mode shapes ($\Psi_i \, (\bar{x})$) for lead-lag and flap bending and $\Theta_i \, (\bar{x})$ for torsion).

The pitch angle due to the root spring is expanded about the equilibrium condition as $\Phi = \Phi_0 + \Delta \Phi \, (\bar{t})$, with no dependence on the blade spanwise coordinate. Also, the inflow expansion coefficients are split into steady-state and perturbation parts as

$$a_n^m (\bar{t}) = \bar{a}_n^m + \tilde{a}_n^m (\bar{t}) \quad \text{and} \quad b_n^m (\bar{t}) = \bar{b}_n^m + \tilde{b}_n^m (\bar{t})$$
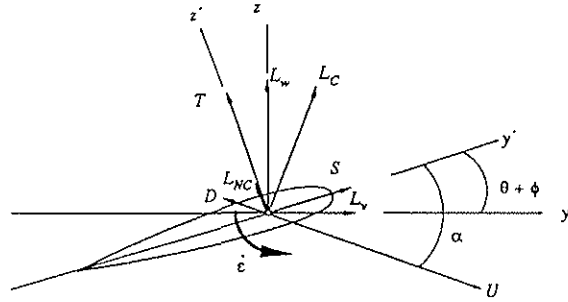
Figure 5. Orientation of Aerodynamic Loads.

Modal Equilibrium Equations

The steady-state part of the inflow equations can be expressed in the following short-hand notation

$$\begin{bmatrix} [B_0][V_0] & -[K] \\ [K]^T & [B_1][V_1] \end{bmatrix} \left\{ \begin{matrix} \{\bar{a}_n^m\} \\ \{\bar{b}_n^m\} \end{matrix} \right\} = \frac{1}{2} \left\{ \begin{matrix} \{\bar{\tau}_n^{mc}\} \\ \{\bar{\tau}_n^{ms}\} \end{matrix} \right\}$$

Since at steady-state the "antisymmetric" part of the pressure (the "sine taus") are zero, the second "row" can be solved for the $\bar{b}$'s as

$$\{\bar{b}_n^m\} = - [V_1]^{-1} [B_1]^{-1} [K]^T \{\bar{a}_n^m\} \quad \text{for } m = 0, Q, 2Q, 3Q, \ldots$$

Then, substituting back in the first "row", a system of S nonlinear algebraic equations is obtained (S is the number of inflow steady-state expansion coefficients taken), that can be represented in the following form

$$\bar{a}_n^m = \bar{a}_n^m \, (V_{0j}, W_{0j}, \Phi_{0j}, \Phi_0, \bar{a}_n^m)$$

As observed in the above representation, the $\bar{a}$'s are nonlinear related to all blade equilibrium generalized coordinates, and to the $\bar{a}$'s themselves. This is a consequence of the use of the nonlinear version of the inflow equations [10], which defines the momentum theory flow parameters as function of the steady, uniform inflow as

$$V_1^0 = V_T = \sqrt{3} \, \bar{a}_1^0; \qquad V_n^m = 2V_T = 2\sqrt{3} \, \bar{a}_1^0 , \quad (n,m) \neq (1,0)$$

Also, the steady-state lift, within the "cosine taus" involves nonlinear relation between flap and lead-lag.

In the blade equations, by substituting only the equilibrium and steady-state quantities and dropping out all time derivative terms, a set of $(3N + 1)$ nonlinear equations for $(\delta V_{0i}, \delta W_{0i}, \delta \Phi_{0i}, \text{ and } \delta \Phi_0)$ is established.

Collecting altogether blade and inflow steady-state equations, a set of $((3N + 1) + S)$ nonlinear algebraic equations in terms of the equilibrium parts of the blade generalized coordinates and the inflow steady-state expansion coefficients $\bar{a}$'s is obtained.

Eigenproblem for the Perturbation Variables

The perturbation equations are obtained by substituting the equilibrium (steady-state) and perturbation quantities, subtracting off the equilibrium (steady-state) equations, and discarding all nonlinear products of dynamic perturbation quantities. The coupled linearized perturbation equations can be set into a state-variable form as shown in Equation (3). In Equation (3), the second "row" comes from the blade perturbation equations and the third "row" is from the unsteady inflow perturbation equations. At the RHS of the equation one can observe the stability matrix; its elements are constant partitioned coefficient matrices which depend on the solution of the equilibrium/steady-state equations. (these matrices are defined in Reference [9]) .The column vector $\{\Delta Z\}$ contains the perturbation modal generalized coordinates from all blades. They are coupled through the inflow pressure functions (Equation (2)), that involve summations over all blades. The stability of small motions about the equilibrium operating condition is determined by the eigenvalues of the stability matrix. It is interesting to observe that by removing last "row" and "column" of

$$\left\{ \begin{array}{c} \{ \varDelta Z \} \\ \{ \varDelta Z^{\bullet} \} \\ \left\{ \tilde{a}_n^m \right\} \\ \left\{ \tilde{b}_n^m \right\} \end{array} \right\}^{*} = \left[\begin{array}{cccc} 0 & I & & 0 \\ -\left[\mathcal{M} \right]^{-1} \left[\mathcal{K} \right] & -\left[\mathcal{M} \right]^{-1} \left[\mathcal{C} \right] & & -\left[\mathcal{M} \right]^{-1} \left[\tilde{k} \right] \\ -\left[\mathfrak{am} \right]^{-1} \left[\mathcal{QS} \right] & -\left[\mathfrak{am} \right]^{-1} \left[\mathfrak{AM} \right] & & -\left[\mathfrak{am} \right]^{-1} \left[q\tilde{s} \right] \end{array} \right] \left\{ \begin{array}{c} \{ \varDelta Z \} \\ \{ \varDelta Z^{\bullet} \} \\ \left\{ \tilde{a}_n^m \right\} \\ \left\{ \tilde{b}_n^m \right\} \end{array} \right\} \tag{3}$$

Equation (3), one basically recovers the same stability problem obtained by Hodges and Ormiston in the 70's [3,2] under a quasi-steady aerodynamic model.

Eigenproblem Solution Approach

To solve for the eigenproblem, a "harmonic-assumed approach" is adopted [9]. Under this solution scheme, one takes advantage of multiblade coordinate transformation, and the equations of motion are written for a reference blade, with the blade modes of vibration (collective, differential, cyclic) assumed beforehand, by keeping selected harmonic numbers in the inflow expansion. This means that the effects of all blades are accounted automatically as the selected harmonic numbers in the inflow expansion are varied.

Taking, for example, a 2-bladed rotor, to obtain the dynamics associated with the collective mode, "even only" harmonic numbers are selected within the inflow expansion (p in the following expressions is any integer),

$$\left\{ \begin{array}{c} \tilde{a}_n^m \\ \tilde{b}_n^m \end{array} \right\} = \left[\left\{ \cdots (\tilde{a}_n^{2p}) \cdots \right\}, \left\{ \cdots (\tilde{b}_n^{2p}) \cdots \right\} \right]^{T}$$

and the vector of blade states takes the form

$$\{ \varDelta Z \} = \left[\frac{\varDelta V_{j1} + \varDelta V_{j2}}{2}, \frac{\varDelta W_{j1} + \varDelta W_{j2}}{2}, \frac{\varDelta \varPhi_{j1} + \varDelta \varPhi_{j2}}{2}, \frac{\varDelta \varPhi_1 + \varDelta \varPhi_2}{2} \right]^{T}, \quad j = 1, 2, 3, \ldots, N$$

Similarly, to obtain the dynamics of the differential (cyclic) mode, one assumes "odd only" harmonic numbers,

$$\left\{ \begin{array}{c} \tilde{a}_n^m \\ \tilde{b}_n^m \end{array} \right\} = \left[\left\{ \cdots (\tilde{a}_n^{2p+1}) \cdots \right\}, \left\{ \cdots (\tilde{b}_n^{2p+1}) \cdots \right\} \right]^{T}$$

and the corresponding vector of blade states takes the form

$$\{ \varDelta Z \} = \left[\frac{\varDelta V_{j1} - \varDelta V_{j2}}{2}, \frac{\varDelta W_{j1} - \varDelta W_{j2}}{2}, \frac{\varDelta \varPhi_{j1} - \varDelta \varPhi_{j2}}{2}, \frac{\varDelta \varPhi_1 - \varDelta \varPhi_2}{2} \right]^{T} \quad j = 1, 2, 3, \ldots, N$$

For a Q-bladed rotor, under the same solution method, the harmonic number varies as

collective mode: $m = 0, Q, 2Q, 3Q, \ldots$

differential mode: $m = \dfrac{Q}{2}, \dfrac{Q}{2} + Q, \dfrac{Q}{2} + 2Q, \ldots \dfrac{Q}{2} + pQ, \ldots$ \qquad (Q even)

cyclic mode: $m = p, Q \pm p, 2Q \pm p, 3Q \pm p, \ldots$

5. Results and Discussion

The rotor configuration and operational conditions for which the results are obtained in this research come from Sharpe's experimental investigations [11] (a two-bladed, untwisted, stiff inplane, torsionally soft hingeless model rotor, including a blade root offset, tested at a nominal angular speed of 1,000 rpm). The hub was designed to allow variation in precone, blade droop, pitch control stiffness and blade pitch angle. Results from the present approach are denoted by GDWM (Generalized Dynamic Wake Model) in the following plots. Values assumed for the harmonic numbers (m) are shown in the legends, where "(E)" means that "even only" harmonic numbers are taken, and "(O)" means that "odd only" harmonic numbers are taken within the inflow expansion. In order to investigate the convergence of the present methodology, the total number of spatial modes (inflow states) in the inflow expansion is chosen as 15, 45, 66, and 91.

Such a selection comes from a mathematically consistent hierarchy presented in Reference [8]. Following this hierarchy and according to solution approach adopted herein, for the steady-state (equilibrium) investigation, "even only" harmonic numbers are taken leading, respectively, to 6, 15, 21, and 28 expansion coefficients (S); for the dynamics analysis, the collective rotor mode needs "even only" harmonic numbers, leading to S equal to 9, 25, 36 and 49, respectively, and the differential rotor mode needs "odd only" harmonic numbers, leading to S equal to 6, 20, 30, and 42, respectively. All results include 5 mode shapes for each of elastic torsion, flap bending, and lead-lag bending deflections. Also, the aerodynamic loads to be presented in this section have been normalized by twice the product of the dynamic pressure at the blade tip and the blade length.

It is important to mention that all the theoretical approaches compared herein have the same structural and inertial models (from References [6] and [3], respectively), so the differences are basically due to the differences in the aerodynamics (that is, in the induced flow and or airloads models).

Steady-State and Equilibrium Results

For this part of the investigation current approach results are correlated with those from the two-dimensional uniform momentum aerodynamics.

Figure 6. Spanwise Steady-State Inflow
$\theta_0 = 8°$; soft pitch flexure, $\beta_{pc} = \beta_d = 0°$

Figure 6 shows predictions for the spanwise distribution of steady-state inflow for the blade at 8° of collective pitch angle (θ_0). The uniform momentum theory takes the inflow at the 3/4 blade span. It predicts too large induced flow at the root sections and too small values at the tip sections. The present approach shows nonuniform inflow distributions, and as the number of expansion coefficients increases, the inflow begins to climb near the blade tip, meaning that they are converging to the Prandtl "exact" tip correction. This characteristic is responsible for the partial capture of the tip relief on both steady-state induced drag and lift to be shown. On the other hand, since this finite-state inflow model is based on a cylindrical, undistorted wake, no upwash due tip-vortex is captured, what would happen if prescribed or free-wake models were used. Since in this case both theories have
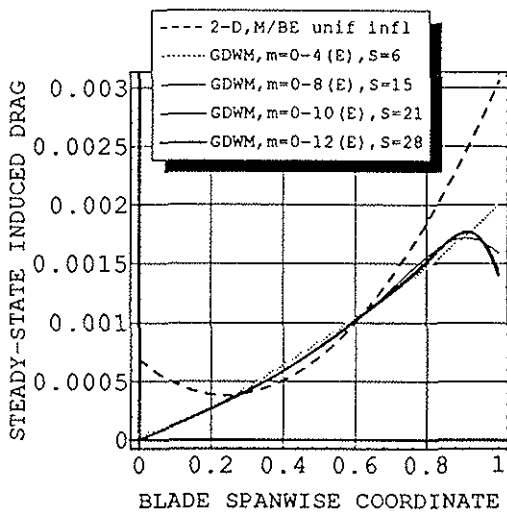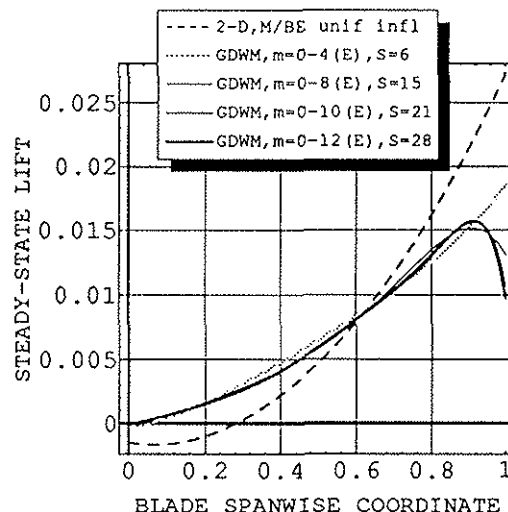
Figure 7. Spanwise Distributions of Steady-State Aerodynamic Loads
soft pitch flexure, $\beta_{pc} = \beta_d = 0°$; $\theta_0 = 8°$; (a) INDUCED DRAG; (b) LIFT

also the exactly same airloads model, the differences in the inflow distributions are the sole responsible for the differences in the predictions of steady-state loads and blade equilibrium deflections.

Figure 7 (a) presents correlations for spanwise nondimensional steady-state induced drag for $\theta_0 = 8°$. Very different predictions are observed from the two models. The present approach captures the three-dimensional tip relief effect as the number of expansion coefficients increases, shown a maximum drag at 92% of the blade span, with sharpe decreasing towards the blade tip. Regarding the two-dimensional momentum approach, too much induced drag is obtained at both blade tip and root sections, which is responsible for large sectional bending moments, leading to higher lead-lag equilibrium deflections, specially near the blade tip, as shown ahead. Correlations for steady-state lift distribu-

tions are presented in Figure 7 (b). Here the two-dimensional momentum results show too small lift at the root and too much lift at the blade tip. Mode shapes for the finite-state inflow approach are qualitatively similar to the ones shown for the induced drag, with more evident three-dimensional tip relief at the blade tip section, though.

Figure 8 (a) shows correlations for lead-lag deflections at the blade tip as function of the collective pitch angle for rotor configurations with no precone or droop and soft pitch flexures. At zero thrust the blade is lagging in the rotor disk plane due to the profile drag. As the thrust gets higher, the blades assume positive chordwise displacements. Since the profile drag is the same in both approaches, the differences observed at high thrust levels are due to differences in the induced drag commented before. Similarly, considerable differences are observed in the flap equilibrium deflections at the blade tip, in almost all range of collective pitch (Figure 8 (b)). They are due to the differences in the lift distributions from the two approaches.
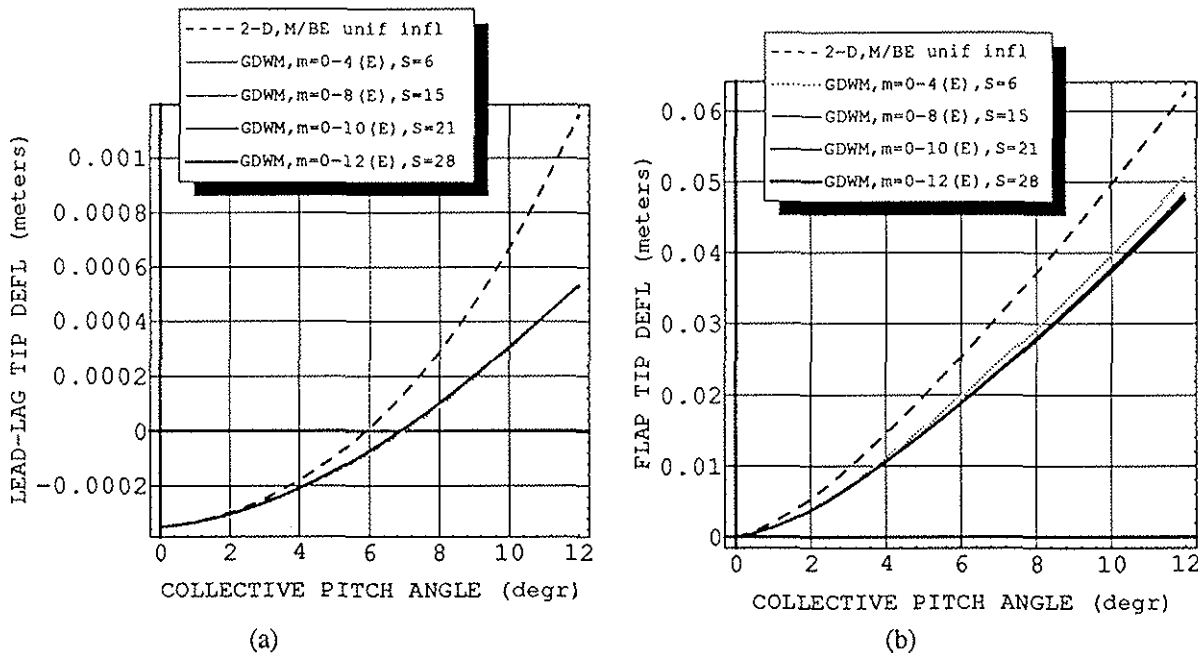
Figure 8. Equilibrium Deflections at the Blade Tip (*m*) vs. Collective Pitch Angle (*degrees*)
soft pitch flexure; (a) LEAD-LAG; (b) FLAP

Just to interpret the displacements results above, taking, for instance, the values of lead-lag and flap at the blade tip at $\theta_0 = 12°$ and computing the inplane displacement, one finds that the blade tip is lagging 0.0052 *m* and is above the rotor disk about 0.048 *m*.

As detailed in Reference [9], relative small differences between the two approaches are obtained for the torsion equilibrium deflections at the blade tip. The role of the pitch flexure in the steady-state results was investigated as well. Aerodynamic loads and blade equilibrium deflections remain practically the same as the stiffness of the pitch flexure is largely varied.

Dynamics Results - Eigenvalue Analysis

In all results to be shown in this section the parameter varied from one equilibrium condition to the next, before small perturbations are applied to the steady-state blade, is the collective pitch angle. Figures 9 to 11 show correlations for the rotor blades in the differential mode of vibration, and Figure 12 shows correlations for the rotor blades in the collective mode of vibration.

For the differential mode, lead-lag damping results are compared with the quasi-steady uniform momentum/blade element aerodynamics from Reference [3], the unsteady three-dimensional panel method from Reference [5] and with the experimental data from Reference [11]; results for lead-lag frequency are compared with the same approaches, except the panel method, whose results are not available.

Figure 9 (a) shows correlations for lead-lag damping as function of the collective pitch angle for blade configurations including soft pitch flexures and zero precone and droop. All theoretical models are based on linear aerodynamics, meaning that no stall effects are included. At low values of collective pitch the damping comes from the profiled drag, that is the same for all models, and one observes that all predictions are approximately the same and close to the experiments. As the absolute value of the collective pitch increases, the large "drop off" observed from the quasi-steady results with respect to experiments starts being captured in part by both the finite-state inflow and panel approaches, which account for unsteady and three-dimensional aerodynamic effects. The rest of the drop is most probably due to increase in drag with angle of attack (recall that the profile drag coefficient is constant in this analysis). Thus,
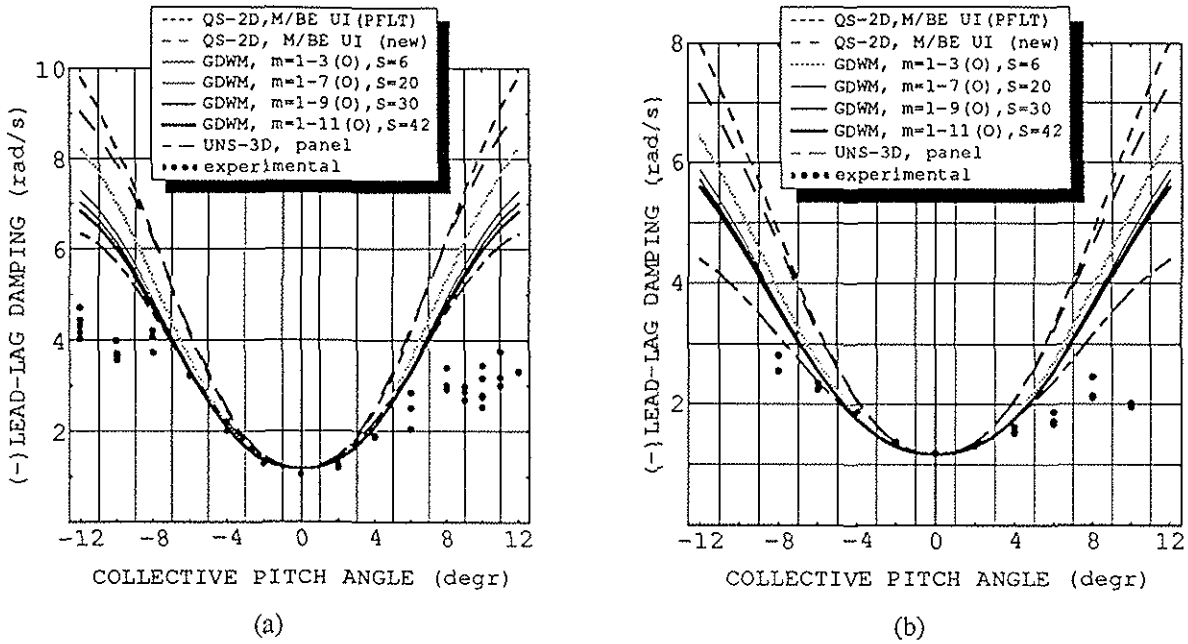
Figure 9. Lead-Lag Damping (*rad/s*) in Terms of Collective Pitch Angle (*degrees*)
Differential Mode of Vibration; $\beta_{pc} = \beta_d = 0°$; (a) SOFT; (b) STIFF pitch flexures

small variations in airfoil shape on the upper and lower surfaces create asymmetric changes in drag, explaining the differences between positive and negative collective pitch in the experimental results. These effects are accentuated at the low Reynolds number, $Re = 600,000$. Also, few corrections in Hodges' previous "PFLT" code and corresponding formulation [3] made in Reference [8] (named "new" in the figure legends) are responsible for some improvements in the predicted values of lead-lag damping for mid-to-high values of collective pitch within the quasi-steady aerodynamics results. Figure 9 (b) presents similar correlations but for the rotor configurations with stiff pitch flexures. Comparing the present approach results with the panel counterparts, one recognizes that, for the soft flexure case, the agreement is very good up to $\theta_0 = 7°$, whereas for the stiff flexures the agreement is very good up to 5°. For values of collective pitch higher than those, the finite-state inflow approach shows larger values of lead-lag damping.

Figure 10 (a) presents correlations for lead-lag damping as function of collective pitch angle for rotor configurations with soft pitch flexures, zero droop and 5° of precone. The best overall correlations with experiments are for the quasi-steady aerodynamics, although the minimum damping value from the experiments is better captured by the panel
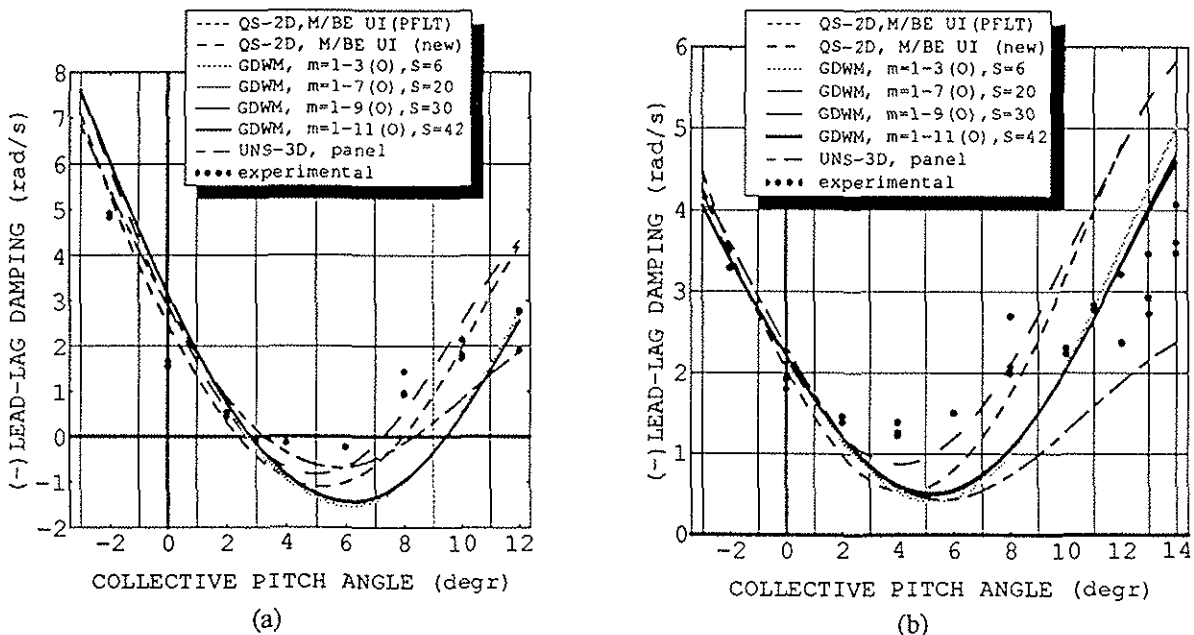

Figure 10. Lead-Lag Damping (*rad/s*) in Terms of Collective Pitch Angle (*degrees*)
Differential Mode of Vibration; (a) soft pitch flexure, $\beta_{pc} = 5°$; $\beta_d = 0°$; (b) stiff pitch flexure, $\beta_{pc} = 0°$; $\beta_d = -5°$
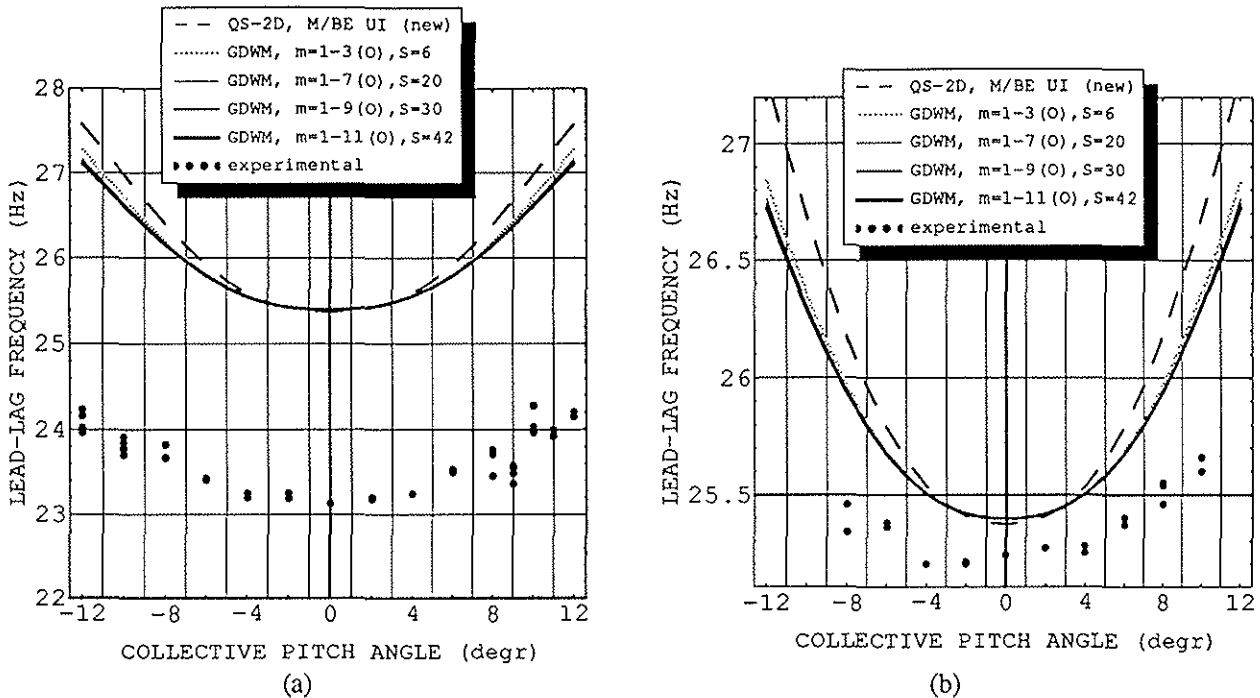
Figure 11. Lead-Lag Frequency (Hz) in Terms of Collective Pitch Angle (*degrees*)
Differential Mode of Vibration; $\beta_{pc} = \beta_d = 0°$; (a) SOFT; (b) STIFF Pitch Flexure

approach. The finite-state inflow results are well converged, and capture the destabilizing effects of positive precone, but the correlations are not satisfactory. Figure 10 (b) shows correlations for rotor configurations with stiff pitch flexures, zero precone, and -5° of droop. The present methodology correlates better with experiments than the panel method, which predicts overly small values of damping at mid-to-high collective pitch.

Figures 11 (a) and (b) show correlations for lead-lag frequency as function of the collective pitch angle for configurations with zero precone and droop, and soft and stiff pitch flexures, respectively. Finite-state inflow results are closer to the experiments for higher values of collective pitch, compared with the quasi-steady results, because the present analysis includes extra inertia from the air mass. Also, very good correlations with the experiments are obtained. At $\theta_0 = 0°$, soft flexure results are 2.27 Hz larger than the experimental results, and 0.16 Hz larger for the stiff pitch flexure configurations. This anomaly raises a question regarding the accuracy of the assumption made in Reference [11] that the pitch flexures were much stiffer than the blade chordwise. Adopting a simple mass-spring system and considering experimental and theoretical results in Figure 11, it turns out [9] that the ratio between blade and flexure chordwise stiffnesses are, approximately, 0.21 and 0.01 for soft and stiff flexure configurations, respectively. This means that the assumption of having only blade flexibility in lead-lag in Sharpe's investigation [11] seems much more accurate for the stiff than for the soft pitch flexure configurations. Similar offsets are found for configurations involving either precone or droop [9].

For the rotor blades in the collective mode of vibration no experimental results are available, so the present approach results are compared to quasi-steady aerodynamics and the panel method. Figures 12 (a) and (b) show correlations for lead-lag damping in terms of collective pitch angle, for rotor configurations with zero droop an precone and with soft and stiff pitch flexures, respectively. One observes that, starting at very low values of the collective pitch, the quasi-steady aerodynamics overpredicts damping. Comparing present approach with thick panel aerodynamics results, for the soft flexure case the agreement is very good up to $\theta_0 = 8.5°$ and for the stiff flexures the agreement is very good up to $\theta_0 = 5.5°$. For values of collective pitch angle higher than those, the finite-state inflow approach shows slight larger values of damping.

Dynamics Results - Eigenvector Analysis

To emphasize the importance of three-dimensional and unsteady effects in the aeroelastic investigations of rotors, correlations for the spanwise distributions of chordwise generalized aerodynamic force (L_v) and of circulatory lift (circulatory L_w) are shown in Figure 13, for the modal frequency correspondent to first lead-lag mode. As observed from Figure 13 (a), at $\theta_0 = 4°$, the present approach predicts a drop of approximately 50% for the chordwise generalized aerodynamic force compared to the quasi-steady aerodynamics results. Due to the predominance of the first lead-lag mode at low thrust levels (low pitch angles) a great part of that represents chordwise damping losses (this confirms that part of the experimental drop-offs in lead-lag damping observed in Figure 9 is due to unsteady, three-dimensional aerodynamic effects). Also, from Figure 13 (b), it is observed a severe drop in the values for the incremental collective and differential circulatory lifts The present approach shows much lower lift fluctuations not
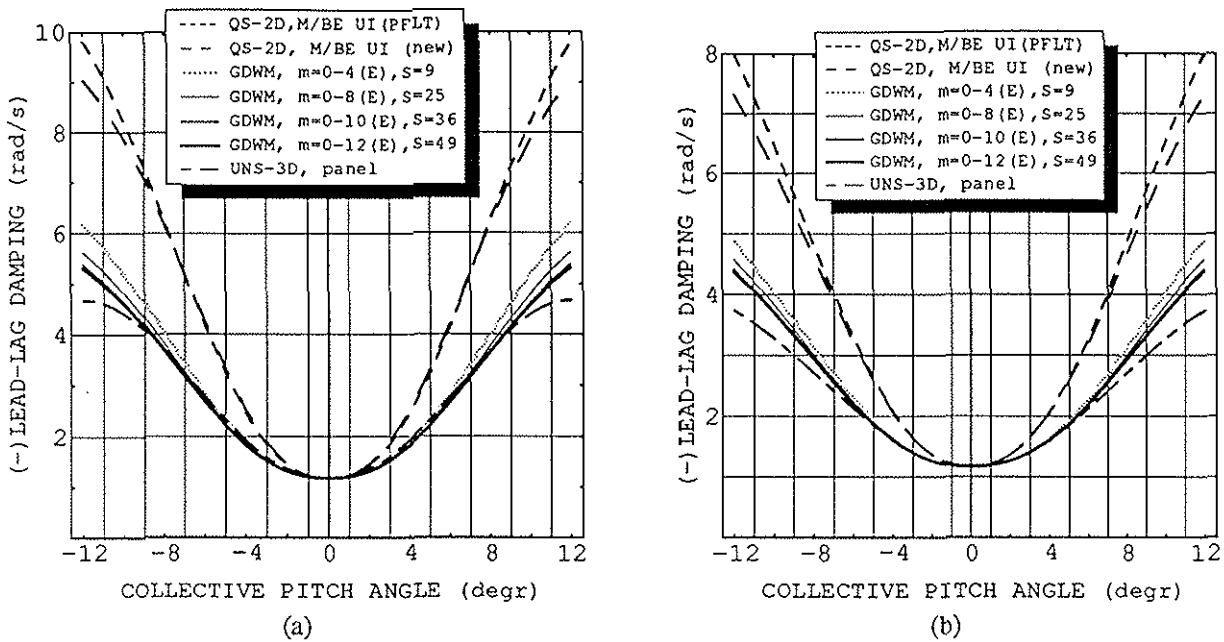
Figure 12. Lead-Lag Damping (*rad/s*) in Terms of Collective Pitch Angle (*degrees*)
Collective Mode of Vibration; $\beta_{pc} = \beta_d = 0°$; (a) SOFT; (b) STIFF Pitch Flexure

only at the tip, which is a three-dimensional tip relief effect, but also at the inboard sections. The integrated value of lift fluctuation from the quasi-steady two-dimensional model is about 2 times the value from the finite-state inflow applications. Concerning the plots in Figure 13, all the eigenvectors are normalized to have the same tip displacement in lead-lag for the comparisons.

As pointed out in Reference [9], for the number of inflow expansion coefficients chosen in this research and for results up to the eigenvalue level, expected savings in CPU range from 16 to 50 times in adopting the present approach instead of the thick panel moving-block analysis. This implies potential applications in rotor optimization.

6. Conclusions

The present research confirms the importance of three-dimensional, unsteady aerodynamics for aeroelastic investigations in hovering flight. The model has been applied to a two-bladed, untwisted stiff inplane hingeless small scale (model) rotor with torsionally soft blades, including a blade root offset, precone, blade droop, pitch control stiffness, and blade pitch angle. The major conclusions of the present study can be summarized as: 1) Numerical results show that three-dimensional tip relief effects within the nonuniform steady-state inflow are significant to predict steady-state aerodynamic loads and blade deflections; 2) Eigenvalue results confirmed the importance of unsteady, three-dimensional aerodynamics in predicting lead-lag damping and frequency, by means of correlations with unsteady three-dimensional thick panel theory and with experiments, and 3) Eigenvector analysis correlations reinforced qualitative and quantitative shortcomings associated with quasi-steady two-dimensional aerodynamic theory for aeroelastic applications in hover. The treatment of the aeroelastic stability through an eigenanalysis as formulated in this work is specially convenient when helicopter integrated dynamics are involved. The elimination of time-marching and moving block analyses, present in current state-of-the-art approaches to the same problem, associated with no essential loss of accuracy for the obtained results, constitutes the primary contributions of the present methodology. The efficiency of this approach makes rotor optimization with aeroelastic stability a practical endeavor.

7. Acknowledgments

8. References

[1] Peters, D.A., and Su, Ay, "An Integrated Airloads-Inflow Model for Use in Rotor Aeroelasticity and Control Analysis", Proceedings of the 47th Annual National Forum of the American Helicopter Society, Phoenix, Az, May 6-8, 1991.

[2] Hodges, D.H. and Ormiston, R.A., "Stability of Elastic Bending and Torsion of Uniform Cantilever Rotor Blades in Hover with Variable Structural Coupling", NASA TN D-8192, April 1976.
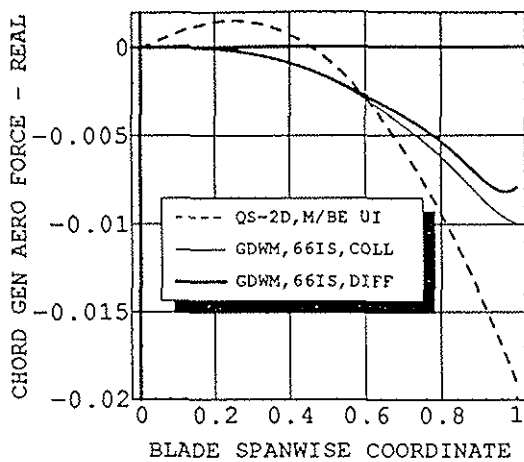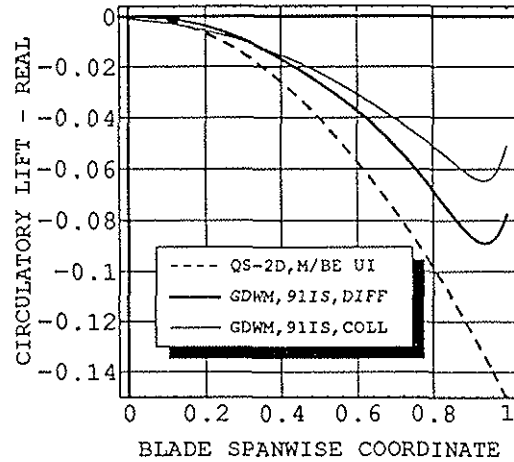
Figure 13. Spanwise Distribution of Generalized Aerodynamic Loads - Collective vs. Differential modal frequency = 1.53/rev; $\theta_0 = 4°$; SOFT PITCH FLEXURE; $\beta_{pc} = \beta_d = 0°$;
(a) CHORDWISE GENERALIZED AERODYNAMIC FORCE; (b) CIRCULATORY LIFT

[3] Hodges, D.H., "Nonlinear Equations of Motion for Cantilever Rotor Blades in Hover with Pitch-Link Flexibility, Twist, Precone, Droop, Sweep, Torque Offset and Blade Root Offset", NASA TM X-73,112, May 1976.

[4] Kwon, Oh Joon, A Technique for the Prediction of Aerodynamics and Aeroelasticity of Rotor Blades, Ph.D. Thesis, Georgia Institute of Technology, December 1988.

[5] Kwon, Oh Joon, Hodges, D.H., and Sankar, L.N., "Stability of Hingeless Rotors in Hover Using Three-dimensional Unsteady Aerodynamics", Journal of American Helicopter Society, Vol.36, No. 2, April 1991, pp. 21-31.

[6] Hodges, D.H. and Dowell, E.H., "Nonlinear Equations of Motion for the Elastic Bending and Torsion of Twisted Nonuniform Rotor Blades", NASA TN D-7818, December 1974.

[7] Peters, D.A. and He, Chengjian, "A Closed Form Unsteady Aerodynamic Theory for Lifting Rotor in Hover and Forward Flight", presented at the 43rd Annual National Forum of the American Helicopter Society, St. Louis, Missouri, May 1987.

[8] He, Chengjian, Development and Application of a Generalized Dynamic Wake Theory for Lifting Rotors, Ph.D. Thesis, Georgia Institute of Technology, July 1989.

[9] de Andrade, D., Application of Finite-State Inflow to Flap-Lag-Torsion Damping in Hover, Ph.D. Thesis, Georgia Institute of Technology, May 8, 1992.

[10] Peters, D.A, and Ninh HaQuang, "Dynamic Inflow for Practical Application", Journal of the American Helicopter Society, Vol. 33 (4), Oct. 1988, pp. 64-68.

[11] Sharpe, D.L., "An Experimental Investigation of the Flap-Lag-Torsion Aeroelastic Stability of a Small-Scale Hingeless Rotor in Hover", NASA TP-2546, January 1986.